The 2004 May 28 Baladeh earthquake (Mw 6.2) in the Alborz, Iran: overthrusting the South Caspian Basin margin, partitioning of oblique convergence and the seismic hazard of Tehran

M. Tatar, J. Jackson, Denis Hatzfeld, E. Bergman

The 2004 May 28 Baladeh earthquake (M_w 6.2) in the Alborz, Iran: overthrusting the South Caspian Basin margin, partitioning of oblique convergence and the seismic hazard of Tehran

M. Tatar,[1] J. Jackson,[2] D. Hatzfeld[3] and E. Bergman[4]

[1] *International Institute of Earthquake Engineering and Seismology,* PO Box 19395/3913, *Tehran, Iran*
[2] *COMET, Bullard Laboratories, Madingley Road, Cambridge,* CB3 0EZ. *E-mail: jackson@esc.cam.ac.uk*
[3] *Laboratoire de Geophysique Interne et Tectonophysique, UJF-CNRS,* 38400 *Grenoble Cedex* 9, *France*
[4] *Department of Physics, University of Colorado at Boulder, Boulder,* CO 80309-0390, *USA*

SUMMARY
We use teleseismic waveform analysis and locally recorded aftershock data to investigate the source processes of the 2004 Baladeh earthquake, which is the only substantial earthquake to have occurred in the central Alborz mountains of Iran in the modern instrumental era. The earthquake involved slip at 10–30 km depth, with a south-dipping aftershock zone also restricted to the range 10–30 km, which is unusually deep for Iran. These observations are consistent with co-seismic slip on a south-dipping thrust that projects to the surface at the sharp topographic front on the north side of the Alborz. This line is often called the Khazar Fault, and is assumed to be a south-dipping thrust which bounds the north side of the Alborz range and the south side of the South Caspian Basin, though its actual structure and significance are not well understood. The lack of shallower aftershocks may be due to the thick pile of saturated, overpressured sediments in the South Caspian basin that are being overthrust by the Alborz. A well-determined earthquake slip vector, in a direction different from the overall shortening direction across the range determined by GPS, confirms a spatial separation ('partitioning') of left-lateral strike-slip and thrust faulting in the Alborz. These strike-slip and thrust fault systems do not intersect within the seismogenic layer on the north side, though they may do so on the south. The earthquake affected the capital, Tehran, and reveals a seismic threat posed by earthquakes north of the Alborz, located on south-dipping thrusts, as well as by earthquakes on the south side of the range, closer to the city.

Key words: continental tectonics, earthquake hazard, earthquakes, Iran, Tehran, seismology, South Caspian Basin.

1 INTRODUCTION

On 2004 May 28 an earthquake of M_w 6.2 occurred near Baladeh in the Alborz mountains of Northern Iran, approximately 70 km north of the capital, Tehran (Figs 1 and 2). Although of only moderate size, it was very significant for two reasons.

First, it was the first earthquake of the modern seismological era to occur near Tehran (Fig. 2), close enough to cause strong ground shaking and widespread panic within the city. Tehran, with its daytime total of about 12 million inhabitants, is widely regarded as one of the most vulnerable urban populations on Earth (e.g. Bilham 2004; Berberian 2005; Jackson 2006). Historical records show that its site was destroyed in previous earthquakes of probable magnitude (M_w) ~ 7 ± 0.5 in the 4th century BC, 855 AD, 958, 1177 and 1830 (e.g. Ambraseys & Melville 1982; Berberian *et al.* 1985). But in those earthquakes the site of Tehran was a much smaller settlement, with a relatively small population, so that casualties were probably

limited to a few thousand. The growth of the modern megacity of Tehran is a 20th century phenomenon, and casualties from a repeat of those earthquakes today would be very much more numerous. The 2006 earthquake was recorded by many strong motion instruments in the Tehran region (http://www.bhrc.ac.ir/Bhrc/d-stgrmo/D-StGrMo.htm) and the performance of many structures was studied in some detail. But for engineers to make effective use of these data it is also important to know the source characteristics of the 2006 earthquake and which fault was responsible; these are the subjects of this paper.

Second, the 2004 earthquake was the first large event to occur in the central Alborz mountains since the 1957 July 2 earthquake (M_s 6.8), for which only rudimentary seismological data are available. The central Alborz form an arcuate, active orogenic belt on the southern margin of the South Caspian Basin (Fig. 1), and accommodate motion between that basin and central Iran. The kinematics, geological structure and evolution of the South Caspian Basin and its
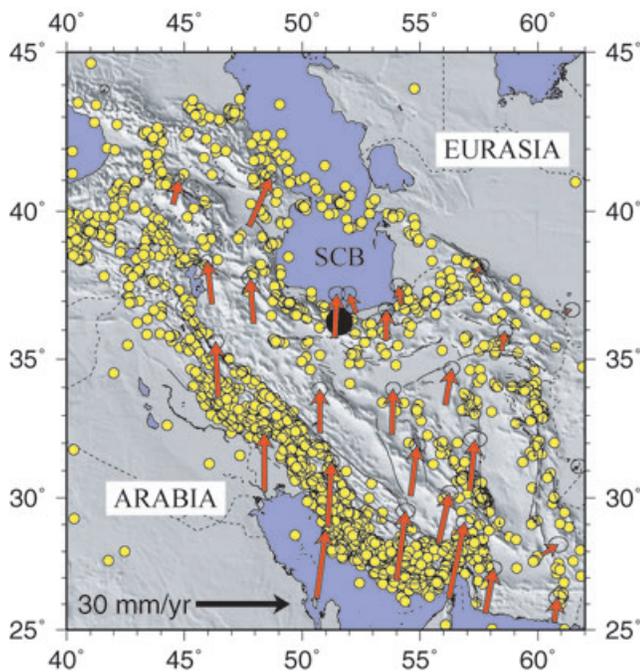
Figure 1. Teleseismically recorded earthquakes in the Iran region in the period 1964–2004 (yellow dots), from the catalogue of Engdahl *et al.* (2006), with the velocities of points in Iran relative to Eurasia determined by GPS (from Vernant *et al.* 2004a) shown by red arrows. The black arrow at the bottom of the map is the velocity scale. Major faults in Iran are shown by thin lines. The epicentre of the 2004 Baladeh earthquake, on the southern margin of the South Caspian Basin (SCB) is marked by a black circle.

surroundings are of intense interest, not least because of their enormous hydrocarbon potential (e.g. Devlin *et al.* 1999). One source of knowledge about the deep structure and kinematics of the active faulting is from earthquake focal mechanisms (e.g. Jackson *et al.* 2002), but little is known from the central Alborz because of the lack of modern earthquakes large enough for detailed seismic waveform analysis, so these topics remain controversial in that region (e.g. Ritz *et al.* 2006). The 2004 earthquake throws important new light on the active tectonics of this southern margin of the South Caspian Basin.

In this paper, we use teleseismic waveform analysis of the 2004 mainshock, together with information from the permanent regional Iranian seismograph networks and from a temporary local network installed to record aftershocks, to form a coherent picture of the coseismic faulting. We then discuss the implications for the seismic hazard of Tehran and the insights this earthquake gives on the deformation of the central Alborz.

2 TECTONIC AND GEOLOGICAL SETTING

At the longitude of Iran most of the ∼25 mm yr^{-1} shortening between Arabia and Eurasia is accommodated within three principal deformation belts; the Zagros mountains in the south, the Alborz mountains on the southern margin of the South Caspian Basin, and the trans-Caspian Apscheron–Balkhan sill in the north (Fig. 1). The South Caspian Basin is thought to be a trapped oceanic remnant (e.g. Berberian 1983), characterized by a high-velocity basement covered with up to 20 km of low-velocity sediments, at least 5 km of which are post upper-Miocene fluvio-deltaic sands that were deposited in about 1–2 Myr years and form the principal offshore hy-
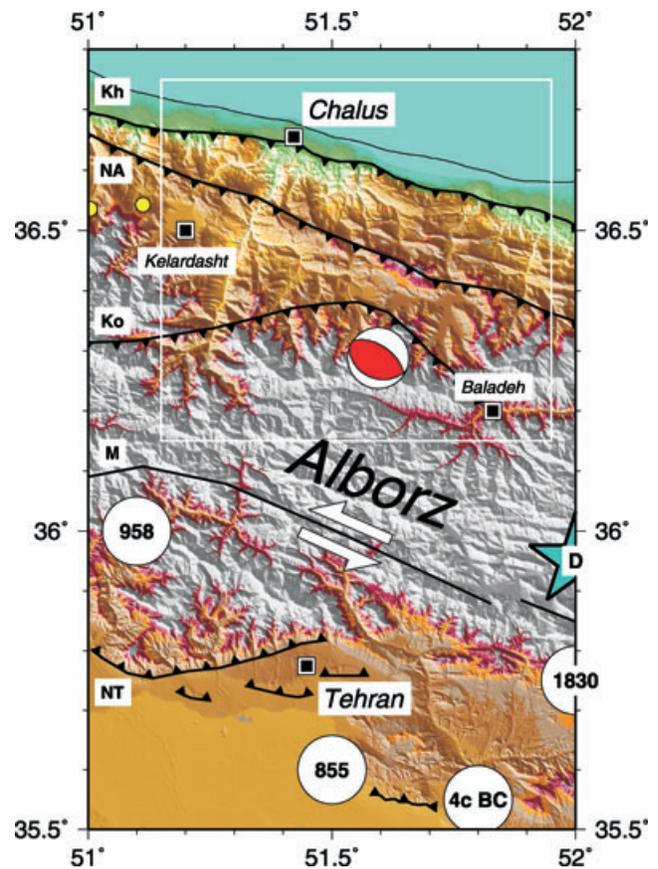

Figure 2. Map of the central Alborz, with SRTM digital topography coloured to emphasize the high mountains (white) and the deep valleys (red) that penetrate the range. The same colour scheme is used in Figs 6 and 9. The lower hemisphere fault plane solution for the 2004 Baladeh earthquake is shown with compressional quadrant in red, positioned at our favoured epicentre (obtained from the HDC cluster analysis; see text). Thrust faults are marked with teeth on the hanging wall as follows: NT for North Tehran Fault, Ko for Kojour fault, Na for North Alborz fault, and Kh for Khazar fault. The left-lateral Mosha fault (M) is marked by a line with no teeth. The blue star (D) is the western edge of the Damavand stratovolcano. White circles show the very approximate estimated centres of the damage regions of the 4th century BC, 855, 958 and 1830 earthquakes, from Ambraseys & Melville (1982). The white box outlines the area of Fig. 6.

drocarbon reservoirs of Azerbaijan and Turkmenistan (see Jackson *et al.* 2002; Allen *et al.* 2002, for a review). A consequence of the rapid sand deposition is that overpressuring of the underlying Oligo–Miocene muds (which are the hydrocarbon source) is common, and manifest as abundant mud volcanoes and diapirs both onshore and in seismic reflection profiles offshore. Post-depositional Late Pliocene and younger folding of the sands has produced many of the hydrocarbon traps, with the folds detaching in the underlying overpressured muds and not affecting the rigid basement at greater depths. The basin is now completely surrounded by active thrust belts, which overthrust its margins, thereby reducing its surface area. From an analysis of the active faulting and earthquake focal mechanisms surrounding the basin, its motion is thought to be roughly NW relative to Eurasia and SW relative to central Iran (Jackson *et al.* 2002). GPS data (Vernant *et al.* 2004b), though limited to a single site on the Iranian Caspian shoreline, suggest the NW velocity of the South Caspian Basin relative to Eurasia is 6 ± 2 mm yr^{-1} and that the motion across the central Alborz involves

roughly 5 ± 2 mm yr^{-1} of shortening and 4 ± 2 mm yr^{-1} of left-lateral strike-slip. Copley & Jackson (2006) estimate a higher value for the South Caspian–Eurasia motion (11 ± 2 mm yr^{-1}) but essentially the same overall motion across the Alborz.

The overall oblique left-lateral motion across the Alborz itself is thought to be spatially separated, or 'partitioned', onto separate strike-slip and thrust faults, both parallel to the trend of the belt. This is seen both in earthquake focal mechanisms (Jackson *et al.* 2002) and in more detailed analysis of the geological structures themselves (Allen *et al.* 2003a; Ritz *et al.* 2006). A curious feature of this partitioning is that the strike-slip faults are in the centre or southern part of the range, in relatively high topography, while the thrust faults occur on both flanks. Thus the largest earthquake of modern times in Iran, the 1990 (M_w 7.3) Rudbar earthquake in the western Alborz, involved $\sim$80 km of left-lateral strike-slip rupture, with the surface trace of the faulting virtually following the drainage divide at elevations of around 2000 m (Berberian *et al.* 1992). Nearer Tehran, the principal strike-slip faulting is on the Taleghan, Mosha (Fig. 2) and Firuzkuh faults, all of which are in the middle of the range, at elevations of 2000–3000 m (Ritz *et al.* 2006; Jackson *et al.* 2002). On the northern flank, the most obvious feature is a line, often called the Khazar thrust on published maps (e.g. Berberian 1983, and Fig. 2), marked by a clear topographic step and an abrupt limit to the incision of drainage (e.g. Antoine *et al.* 2006), though geological and geomorphological details are obscured by the high erosion and dense vegetation, both consequences of extreme rainfall. The precise nature of this structure, and whether it is a fold above a blind thrust (Allen *et al.* 2003a) or even exists as a thrust at all (Guest *et al.* 2006a) are debated. The southern flank is marked by the abrupt step of the North Tehran Fault and its associated foreland faults. Here, in the much drier climate, the morphology is much better preserved, and several co-seismic scarps attest to the Holocene activity of this thrust-fault system (Berberian *et al.* 1985; Nazari *et al.* 2007).

The present day configuration and rates of faulting in the Alborz were probably established around 5 Ma ago (Allen *et al.* 2004; Axen *et al.* 2001). The earlier geological history of the Alborz is of less importance for this paper, though recent summaries can be found in Axen *et al.* (2001), Allen *et al.* (2003b), Vincent *et al.* (2005), Guest *et al.* (2006a,b) and Zanchi *et al.* (2006).

The region of Fig. 2 is remarkable for the almost total absence of teleseismically recorded earthquakes from 1964 until the Baladeh earthquake in 2004. Only two events are listed in Engdahl *et al*'s (2006) updated catalogue, of m_b 4.7 and 4.4 in 1973 and 1993, shown by yellow circles in Fig. 2. The destructive earthquake of 1957 July 2 (M_s 6.8) occurred just east of Fig. 2 ($\sim$36.05°N 52.45°E) and was the only significant earthquake in the region for the last 100 yr (Ambraseys & Melville 1982). A poorly constrained first-motion fault-plane solution is sufficient to show it probably involved thrust faulting, with a strike parallel to the belt (McKenzie 1972), but there was no reported surface faulting to confirm this. The principal historical earthquakes that devastated the Tehran region in the 4th century BC, 855 AD, 958 and 1830 are shown in Fig. 2, but their locations are very schematic, reflecting an estimate of the centre of their main damage regions (Ambraseys & Melville 1982; Berberian *et al.* 1985); they are not formal epicentres, and could be in error by up to 50 km. The 1177 earthquake, which also devastated the historic Tehran site, was probably located a little west of Fig. 2 ($\sim$35.7°N, 50.7°E). The well-known occurrence of these events on the south side of the Alborz has caused modern studies of the seismic hazard of Tehran to focus mostly on the Mosha and North Tehran fault systems. The region of Fig. 2 is, nonetheless, characterized by a high level of microearthquake activity, which is recorded by various semi-permanent networks around Tehran (Ashtari *et al.* 2005).

An issue of particular significance concerns the focal depths of earthquakes in the Alborz. In the western Alborz and Talesh (the N–S coast of the SW corner of the South Caspian Basin) teleseismic waveform modelling of moderate-sized earthquakes reveals centroid depths of up to $\sim$27 km, indicating the eastward overthrusting of the South Caspian Basin on low-angle thrusts dipping 10–20° towards the land (Jackson *et al.* 2002). East of $\sim$49°E existing teleseismic waveform modelling had confirmed nothing deeper than $\sim$15 km within the Alborz, a much more typical depth range for Iran, yet local networks (Ashtari *et al.* 2005) and a few teleseismic locations (Engdahl *et al.* 2006) suggested some earthquakes were as deep as 25–30 km in the central and eastern Alborz as well. In this respect too, the 2004 Baladeh earthquake is informative because, as we will show, it had a centroid at $\sim$22 km and aftershocks that extended to about 35 km depth.

3 EFFECTS OF THE BALADEH EARTHQUAKE

The Baladeh earthquake, also known as the Baladeh–Kojour earthquake in Iran, occurred at 12:38 GMT (17:08 local time) in a relatively sparsely populated mountainous area in late-afternoon, when many people were outdoors. For these reasons, casualties were relatively light for an event of this size in Iran, with approximately 35 people killed and 400 injured. Some of those deaths were caused by landslides and rockfalls on the Chalus–Tehran road, one of the principal trans-Alborz communication arteries. Landslides were common in the steep topography of the epicentral region, but no evidence of co-seismic surface faulting was discovered; a result that we show below is not surprising (in retrospect), given the depth and source dimensions of the faulting. The epicentral region is one of high rainfall, dense vegetation and frequent landslides due to the steep topography, so that we were unable to obtain information from radar interferometry as coherence between images is very poor. No dense GPS networks were available at the time. The only accessible information on coseismic faulting is therefore from seismology.

The earthquake was strongly felt in Tehran 60–70 km away, causing some panic and anxiety in the population, especially as they were anxious about earthquakes following the 2003 Bam catastrophe, which occurred 5 months earlier, killing $\sim$40 000 people (Jackson *et al.* 2006). Strong motion instruments in Tehran recorded accelerations of about 6% g on horizontal and vertical components. The nearest instrument to the epicentre, about 10–20 km distant to the NE at Poul (Kojour), recorded horizontal and vertical accelerations of $\sim$30% g and 26% g (BHRC 2004).

4 TELESEISMIC WAVEFORM ANALYSIS

The 2004 Baladeh earthquake was widely recorded by stations of the Global Digital Seismic Network (GDSN) and the fault parameters of its centroid are well determined by long-period *P* and *SH* body waves. We first convolved the digital broad-band records from stations in the teleseismic distance range of 30–90° with a filter that reproduces the bandwidth of the old WWSSN 15–100 long-period instruments. At these wavelengths, the source of an earthquake this size appears as a point in space (the centroid) with a finite rupture time, and the resulting seismograms are sensitive to the source parameters of the centroid while relatively insensitive to the details of geological structure. We then used the MT5 version (Zwick

et al. 1994) of McCaffrey & Abers's (1988) and McCaffrey *et al.* (1991) algorithm, which inverts the *P* and *SH* waveform data to obtain the strike, dip, rake, centroid depth, seismic moment and the source time function, which is parameterized by a series of isosceles triangle elements of half-duration τ s. We always constrained the source to be a double-couple. Stations are weighted by azimuth density, and then the weights of *SH* waveforms are halved to compensate for their generally larger amplitudes. The method and approach we used are described in detail elsewhere (e.g. Nábělek 1984;

McCaffrey & Nábělek 1987; Molnar & Lyon-Caen 1989; Taymaz *et al.* 1991) and are too routine to justify detailed repetition here.

P and *S* onsets were unusually impulsive on the broad-band records for this earthquake, so arrival times of these phases could be read accurately and used to align the observed and synthetic long-period seismograms. The observed and synthetic seismograms for the 'best' minimum-misfit source parameters found by the inversion process are shown in Fig. 3. Nodal planes for both *P* and *SH* are well-determined by the wide azimuth distribution of the recording
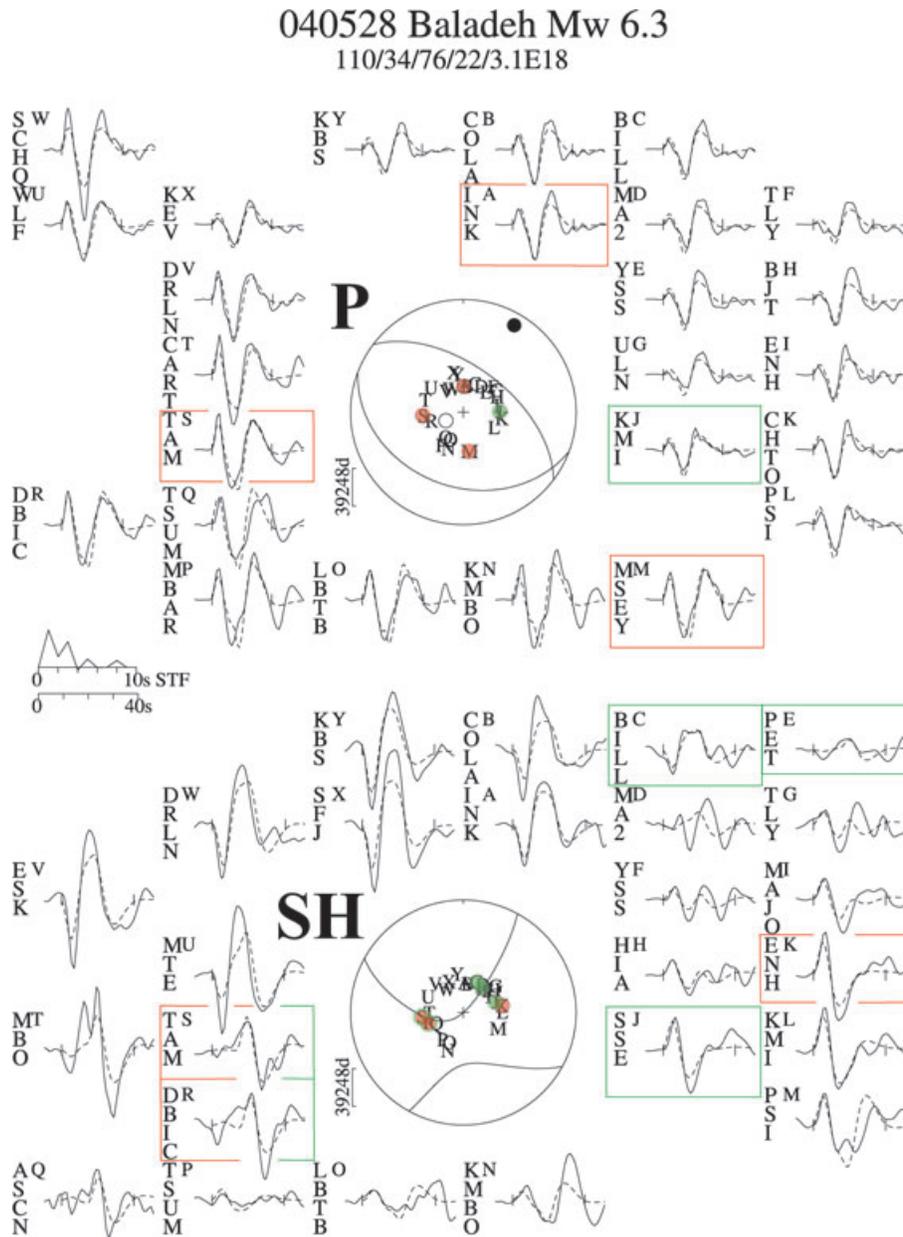

Figure 3. *P* and *SH* waveforms for the 2004 Baladeh earthquake. The event header shows the strike, dip, rake, centroid depth and scalar seismic moment (in N m) of the minimum misfit solution. The top focal sphere shows the lower hemisphere stereographic projection of the *P* waveform nodal planes, and the positions of the seismic stations used in the modelling routine. The lower focal sphere shows the *SH* nodal planes. Capital letters next to the station codes correspond to the position on the focal sphere. These are ordered clockwise by azimuth, starting at north. The solid lines are the observed waveforms, and the dashed lines are the synthetics. The inversion window is marked by vertical lines on each waveform. The source time function (STF) is shown, along with the time scale for the waveforms. The amplitude scales for the waveforms are shown below each focal sphere. The *P* and *T* axes within the *P* waveform focal sphere are shown by a solid and an open circle, respectively. Synthetic seismograms were calculated in a half-space of V_p 6.5 km s^{-1}, V_s 3.7 km s^{-1} and density 2.8 gm cm^{-3}. Green and red boxes outline stations used in Figs 4 and 5, respectively, with green and red dots showing their locations on the *P* and *SH* focal spheres.
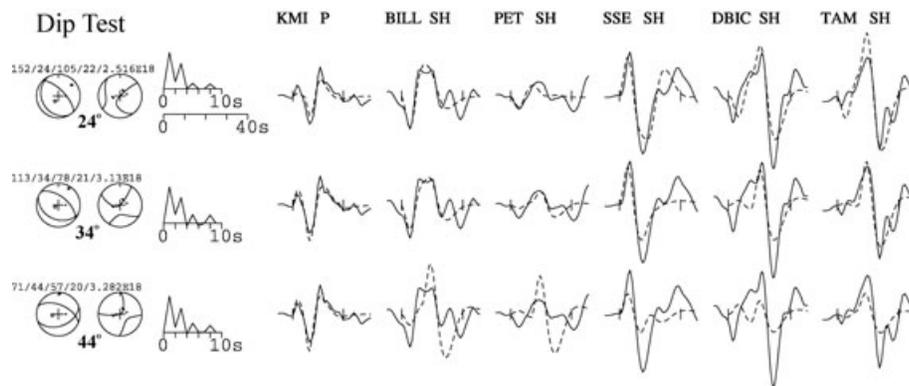
Figure 4. Tests to illustrate the resolution of dip. Observed (solid) and synthetic (dashed) seismograms are shown for *P* waves at KMI and *SH* waves at BILL, PET, SSE, DBIC and TAM, all outlined by green boxes in Fig. 3. The formal best fit inversion was for a dip of 34° (middle line). In the top line the dip was fixed at 24°, and in the bottom it was fixed at 44°; all other source parameters were free to change in the inversion which then yielded the synthetic seismograms shown. *P* (left) and *SH* (right) focal spheres are shown for the resulting solution, which is also summarized above them in the same notation as in Fig. 3 (strike, dip, rake, depth, moment). The column to the right of the focal spheres shows the source time function in each case. The inversion window is marked by vertical ticks. See text for discussion.

stations, and the waveforms show a relatively simple source time function of 4–6 s duration. As will become clear in later discussion, it is probable that the nodal plane dipping SW is the fault plane, which has a strike of 110°, a dip of 34°, and a rake of 76°. The centroid depth is 22 km and the moment is 3.1×10^{18} Nm (M_w 6.3).

Of particular interest in the discussion that follows are the centroid depth and the dip. To investigate the uncertainties in these parameters, we carried out a number of tests, in which the parameter under investigation was held fixed at various values either side of the 'best-fit' value, while the other parameters we allowed to vary, to minimize the misfit. In this way, we were able to see how much the parameters can be changed before there is a substantial deterioration in the fit between observed and synthetic seismograms. This, too, is now a routine procedure (see Molnar & Lyon-Caen 1989; Taymaz *et al.* 1991). An illustration of the sensitivity to dip is shown in Fig. 4, in which the stations that have been chosen are highlighted by green boxes in Fig. 3. If we fix the dip at values 10° greater or less than the minimum misfit solution of 34°, the inversion compensates by trading-off rake against strike. It does this because the small onsets of *P* waves in the NE requires them to be near the NE-dipping (auxiliary) nodal plane, whose orientation does not change much. As a result, *P* waves are not much affected (e.g. wave-

forms at KMI in Fig. 4) as the stations all remain near the centre of the *P*-wave compressional quadrant on the focal sphere. But the *SH* waveforms are much more sensitive to these changes. All those in Fig. 4 are significantly worse-fitting with a dip of 44° (line 3) than with the dip of 34° (line 2). At 24° the fit is not so degraded, and the fit at some stations (e.g. DBIC) may even be improved, but the fit of amplitudes at several stations (e.g. TAM) is worse, and the resulting misfit residual is greater. We conclude that the dip could be up to 10° shallower than 34°, but not more than 5° steeper.

A test showing the sensitivity to depth is given in Fig. 5, with the depth fixed at values 10 km shallower and deeper than the minimum misfit solution of 22 km. Stations used are outlined by red boxes in Fig. 3. This test shows the expected trade-off between depth and the duration of the source time function, with longer durations associated with shallower depths (line 1) and shorter durations with deeper (line 3). This trade-off leads also to a trade-off with moment as, at shallow depths the interference of direct and surface-reflected rays reduces the amplitude and a correspondingly greater moment is necessary to produce the amplitude of observed seismograms. Thus line 1 has a greater moment (5.0×10^{18} N m) and line 3 a smaller moment (2.3×10^{18} N m) than the minimum misfit value of 3.1×10^{18} N m. These trade-offs do not greatly affect the fit of *P* waves at depths less than about 25 km, but at greater depths, the waveform

Figure 5. Tests to illustrate the resolution of centroid depth, in the same format as Fig. 4, but using different stations, outlined by red boxes in Fig. 3. The formal best fit inversion was for a depth of 22 km (middle line).In the top line the depth was fixed at 12 km, and in the bottom it was fixed at 32 km; all other source parameters were free to change in the inversion which then yielded the synthetic seismograms shown. See text for discussion.

cannot be short enough, however short the source time function (see INK in Fig. 5). The effect on *S* waves is much greater at stations DBIC and TAM, which are close to an *SH* nodal plane in the SW. At these stations, a small direct *S* wave is followed by a much larger sS surface reflection, and the separation between them is clearly visible on the seismograms. This feature alone is sufficient to fix the centroid depth at 22 ± 4 km. This depth is in good agreement with the 27 km reported by the United States Geological Survey and Engdahl *et al.* (2006), based on a visual identification of *pP* on broad-band seismograms.

After similar tests for strike and rake, we estimate the uncertainties in source parameters to be ±20° in strike, −10/+ 5° in dip, ±25° in rake, ±4 km in depth and ±15 per cent in moment. The relatively large uncertainties in strike and rake are for the SW-dipping nodal plane, which we expect to be the fault plane (see below). The steeper NE-dipping nodal plane is better defined. If this is the auxiliary plane, its strike, which varied by less than ±10° in our tests, defines the slip vector azimuth, which is therefore 036 ± 10°.

5 MAINSHOCK EPICENTRE

It is obviously important to constrain the nucleation point ('hypocentre') of the mainshock as well as possible. Although a temporary local network was installed immediately after the earthquake to record aftershocks, at the time of the mainshock itself, only the sparse stations of the permanent Iranian networks and teleseismic or regional stations that report to the International Seismological Centre were available. Epicentres in Iran that are based on teleseismic and regional arrival times alone are known to be in error by up to 10 km or more, even for well recorded earthquakes (e.g. Engdahl *et al.* 2006; Jackson *et al.* 2006), and hypocentral depths are generally even more uncertain.

We show five estimates of the mainshock epicentre in Fig. 6 and Table 1. In blue is the best estimate based on teleseismic and regional arrival time data, by Engdahl *et al.* (2006). In green is the estimate from the Institute of Geophysics at Tehran University (IGTU), based on their permanent network of stations in the Alborz, which however are all south of the epicentre. In white, we show two relocated epicentres using arrival times, which we read ourselves, at all available regional stations up to 300 km. We then relocated the hypocenter using a crustal velocity structure determined by 1-D inversion of traveltimes in the local temporary network. We used a mantle velocity 8.0 km s^{-1} which was determined by Ashtari *et al.* (2005) from 2 years of seismicity in the regional permanent network. The Moho depth is certainly not constant across the Alborz and we took a mean value of 40 km, a value between the receiver function results south of the Alborz (Sodoudi *et al.* 2004) and those beneath the Alborz (A. Paul, personal communication 2006). The two epicentres shown are those obtained using *P* arrival times only (white square) or *P* and *S* arrival times (white circle); see Table 1. The rms residuals of 0.33 s and 0.31 s are comparable with the accuracy of the arrival times, which is no better than 0.5 s. The formal uncertainties in these two epicentres are about 3 km, but the true accuracy is almost certainly worse.

Finally, we established the hypocenter of the 2004 Baladeh mainshock using a recently developed method based on multiple-event location of a cluster of earthquakes containing one or more 'calibration' events that have been well located by a local seismograph network. This is probably the best of the various locations in Table 1, and the procedure for obtaining it must be described in some detail. The key to calibration locations is to keep path lengths (thus, theoretical traveltimes) short and have good azimuthal cov-
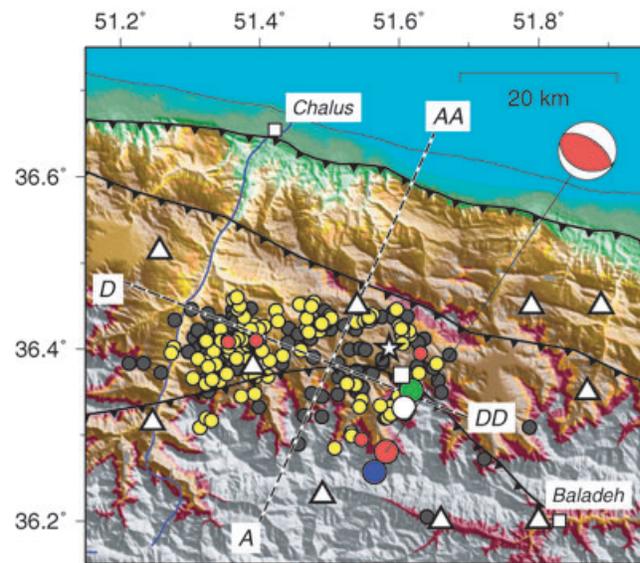

Figure 6. The epicentral area of the 2004 Baladeh earthquake (the white box in Fig. 2), showing the high-quality aftershock locations (group A) in yellow, and lower-quality locations (group B) in gray. White triangles are temporary seismograph stations, and the white star is the strong-motion instrument at Poul (Kojour). Mainshock epicentre estimates are the large circles in blue (from the catalogue of Engdahl *et al.* 2006), green (from the Institute of Geophysics at Tehran University), red (from the HDC cluster analysis reported here, and white from *P* (square) or *P* and *S* (circle) arrival times at regional Iranian stations: see Table 1. The smaller red circles are four aftershocks that were also located by HDC cluster analysis. The formal uncertainties in the yellow and red epicentres are about twice the size of their respective circles. The red focal sphere is that of the mainshock, as in Fig. 2. The faults shown are the Khazar (north), North Alborz (middle) and Kojour (south): see Fig. 2. A–AA and D–DD are the lines of the cross-sections shown in Fig. 7.

Table 1. Hypocentral determinations of the Baladeh mainshock of 2004 May 28 (12:38 GMT), by R. Engdahl (2006), the Institute of Geophysics at Tehran University (IGTU), the HDC cluster analsyis described in this paper, and from regional Iranian stations in the Alborz mountains using arrival times of just *P* waves (15 phases used; distance to closest station 59 km; rms 0.33 s) or both *P* and *S* waves (23 phases, 58 km, 0.31 s, respectively). The HDC depth of 20 km was fixed in the analysis, not determined by it.

Symbol Figs 6, 7 and 9	Source	Lat. °N	Long. °E	Depth km
Blue circle	Engdahl *et al.* (2006)	36.257	51.565	27
Green circle	IGTU	36.352	51.618	8
Red circle	HDC cluster	36.281	51.582	20
White square	Iranian *P*	36.370	51.603	20
White circle	Iranian *P+S*	36.332	51.607	25

erage. Epicentral distances must be kept less than 150–250 km in most regions (e.g. Bondar *et al.* 2004). This method is well suited to the study of mainshock–aftershock sequences when a dense local network can be installed shortly after the mainshock, as it was for Baladeh (see Section 6). The calibration events must be large enough to be well recorded at regional and teleseismic distances, for phase arrival times at these distances are utilized in the multiple event relocation analysis to constrain the relative locations of all events in the cluster. In this way, the mainshock is linked to one or more aftershocks with locations known to high accuracy. The method of multiple event location used here is the Hypocentroidal

Table 2. The two calibration earthquakes used in the HDC location analysis, followed by the final adjusted locations of the mainshock (at 12:38 GMT) and four aftershocks; all shown in red in Fig. 6. All depths were fixed, and not determined by the location procedure.

Date	Origin time	Latitude	Longitude	Depth
Calibration locations:				
2004.05.29	0923:48.59	36.438	51.383	16.0
2004.05.30	1927:00.77	36.388	51.624	10.0
Final HDC locations:				
2004.05.28	1238:45.85	36.281	51.582	20.0
2004.05.28	1315:08.31	36.295	51.546	20.0
2004.05.28	1947:04.03	36.410	51.395	15.0
2004.05.29	0923:49.32	36.408	51.355	16.0
2004.05.30	1927:00.61	36.395	51.631	10.0

Decomposition method (HDC), introduced by Jordan & Sverdrup (1981). Other applications of the calibration method using HDC are presented by Walker *et al.* (2005), Parsons *et al.* (2006) and Biggs *et al.* (2006).

The cluster of earthquakes used for this study was taken from the updated EHB catalogue (Engdahl *et al.* 2006), using events within about 50 km of the mainshock. Because of the low level of seismicity in the area over the past few decades, the cluster contained only 12 events, including the 2004 Baladeh mainshock and four of the larger aftershocks. Two of these aftershocks (May 29 at 0923 hrs, m_b 4.7, and May 30 at 1927 hrs, m_b 4.4; Table 2) were well located by the temporary network, and were used to calibrate the absolute location of the cluster. Using the *P* and *S* phase arrival times of the temporary stations and some of the closer permanent Iranian stations (no station farther than 1.9 degrees), we first located the two calibration events. The velocity model described in Section 6 was used. The temporary stations have epicentral distances in the range of 10–40 km from the epicentres, providing good depth control. The calibration locations are given in Table 2.

The HDC analysis of the cluster, using regional and teleseismic arrival times, provides strong constraints on the relative locations and origin times, but the absolute location of the cluster (defined by the location of the geometric mean or hypocentroid of the cluster events) is expected to be biased by unmodelled Earth structure, as with any method of teleseismic location. Because the HDC analysis is not very sensitive to focal depth, we fixed all depths according to waveform depths (Section 4) or the most accurate nearby aftershock locations. Thus to calibrate the cluster, we shift it in space and time (keeping relative locations and origin times constant) to best match the locations and origin times of the calibration events. Having two calibration events give us a check on internal consistency of the calibration shift. We propagate uncertainties of relative locations with uncertainties of the calibration locations to estimate an overall uncertainty in the necessary calibration shift. The locations from the HDC analysis for the 2004 Baladeh mainshock and four aftershocks are shown in Table 2 and in red in Fig. 6. The formal (90 per cent) uncertainty in the calibrated epicentre of the mainshock is roughly a circle of 3 km radius.

All five epicentres are relatively restricted in space, at the eastern end of the aftershock pattern (Section 6), and are aligned in a direction roughly 020°, which is perpendicular to both the strike of the mainshock fault plane (110°) and of the Alborz mountains as a whole. The red (HDC) and blue (EHB) estimates, which use teleseismic data, are about 3 km apart and about 7 km SSW of the group (white and green) that are based entirely on local or regional Iranian data, and which certainly suffer from a one-sided local sta-

tion distribution, with all or most stations located south, or SSW, of the epicentral region.

The closest strong-ground motion station which recorded the mainshock was at Poul (Kojour), marked by a white star in Fig. 6. According to the report by BHRC (2004), this station recorded an *S-P* time of 2.5 s, corresponding to a hypocentral distance of ~20 km. It is located almost in line with the five mainshock estimates in Fig. 6 and could potentially be used to help discriminate between them. However, its hypocentral distance is similar to the probable hypocentral depth (based on the mainshock centroid and aftershock depths discussed below). As a result, and since the hypocentral depth is probably no better than ±10 km in all five mainshock locations in Fig. 6 and Table 1, the actual use of Poul as a discriminant is limited (Fig. 7): it could be made to be 'consistent' with nearly all of them.

6 LOCAL RECORDING OF AFTERSHOCKS

Within 24 hr of the mainshock, a temporary seismograph network of 10 stations had been installed to record aftershocks. It consisted of 3-component CMG6TD (Guralp) stations recording at a rate of 125 sps, with timing controlled by GPS. This network was maintained for three weeks, ending on July 19.

The data were analysed in the manner described by Tatar *et al.* (2005), for the study of the 2003 Bam aftershocks. First we determined a V_p/V_s ratio of 1.782 ± 0.006 by averaging the differences between 570 *S* and *P* arrival times for earthquakes recorded by a minimum of 8 stations. Second, we searched for an appropriate 1-D velocity structure by inverting the arrival times (Kissling 1988) of a selected set of earthquakes (with rms residual less that 0.2 s, horizontal and vertical errors less than 2 km and more than 8 recording stations). Since the resulting structure could depend on the starting model, we began with an initial structure comprising a stack of 2-km-thick layers to detect the main interfaces, and limited the number of unknowns by using a 3-layer model over a half-space. The 3-layer starting model was randomly perturbated to ensure convergence to a final model. The model used here was:

Layer	V_p km s^{-1}	V_s km s^{-1}	Depth to top km
1	5.60	3.15	0
2	5.80	3.26	12
3	6.40	3.60	14
hs	8.10	4.55	35

The aftershocks were then located using the HYPO71 routine (Lee & Lahr 1972). In discussing the locations of these aftershocks, we have split them into two groups, based on the quality of their hypocentre determinations. Group A is the best located, and consists of 122 earthquakes, all of which have at least 8 arrival times (either *P* or S) in their determinations, with rms residuals of ≤0.2 s, and formal horizontal and vertical errors of less than 2 km. Group B consists of a further 125 earthquakes, making a total of 247, all of which have a minimum of 4 *P* or *S* arrival times in their determinations.

6.1 Epicentres

The epicentres of the locally-recorded aftershocks are shown in Fig. 6, which includes both the high-quality group A locations (yellow) as well as the less good group B locations (in gray). The pattern
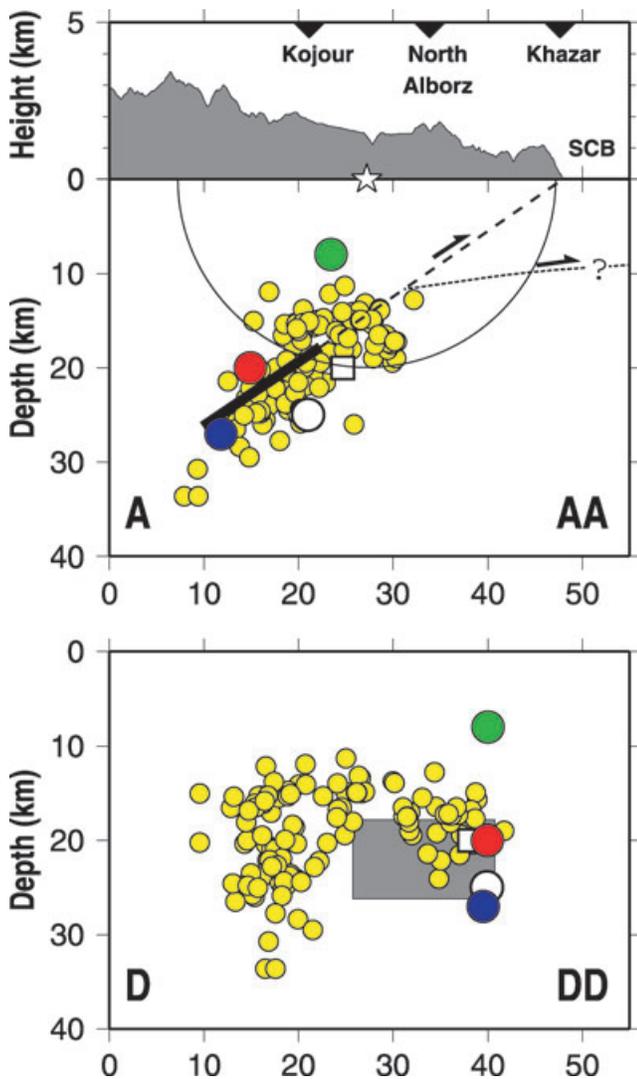
Figure 7. Sections A–AA (top) and D–DD (bottom) through the aftershock locations; see Fig. 6 for the lines of the sections. Aftershock locations (yellow circles) are only shown for the high-quality group A events, whose formal uncertainties in horizontal and depth positions are both less than 2 km. In the section, transverse to strike (A–AA) the large blue, red, green and white circles, and white square, are the mainshock hypocentres estimates in Fig. 6, projected onto the section: all of them have depths that are uncertain by up to ~10 km. The thick black line is the projection of a fault plane with down-dip width 15 km, with the orientation of the SW dipping nodal plane in Fig. 3, centred at 22 km depth (the teleseismic centroid). A thinner dashed line shows the 'Khazar thrust' projected downwards from the surface at the same dip; though whether such an upward continuation of the coseismic fault at the same dip is a splay off a flatter fault entering the South Caspian basin (schematically indicated, at an arbitrary depth, by a dotted line marked ?) is uncertain. The topography along section A–AA is plotted at the top (note the vertical exaggeration), with the surface outcrop positions of the Kojour, North Alborz and Khazar faults marked by arrows. SCB is the South Caspian Basin. The white star is the location of the Poul strong-motion station, projected onto the section. Its hypocentral distance, based on a reported *S*–*P* time of 2.5 s, is about 20 km, shown by the circle of that radius centered on the station. In the longitudinal section (D–DD) the same estimated co-seismic fault plane is shown in gray and with the same mainshock hypocentral projections as in section A–AA. See text for discussion.

is quite confined in space to a region about 40 km along strike and 20 km across strike, and is well-positioned in the middle of the station distribution. All the earthquakes are on the north side of the Alborz, between the high peaks of the drainage divide and the Caspian Sea, and nearly all of them are located along-strike to the WNW from the mainshock epicentre estimates. The true mainshock epicentre is therefore likely to lie in the SE corner of the aftershock pattern. The four smaller red circles in Fig. 6 include two early aftershocks on May 28, at 12:38:45.8 and 13:15:08.6 GMT (Table 2), which occurred before the temporary seismic network was installed. Their epicentres were determined in the same HDC cluster analysis used for the mainshock, and clearly lie within the main aftershock pattern. It is also notable that the aftershock pattern ends in the west in the valley of the north-draining Chalus river, one of the principal drainages of the Alborz range.

6.2 Depths

Fig. 7 shows across-strike (A–AA) and along-strike (D–DD) sections through the aftershock pattern, in which only the high-quality group A locations are included. These all have formal errors in depth less than 2 km; about the size of the yellow circular symbols. Several characteristics of this depth distribution are notable.

First, the pattern is confined to depth range 10–35 km (see also Fig. 8). The deeper earthquakes are unusually deep for Iran, where most seismicity is shallower than 20 km. But other earthquakes
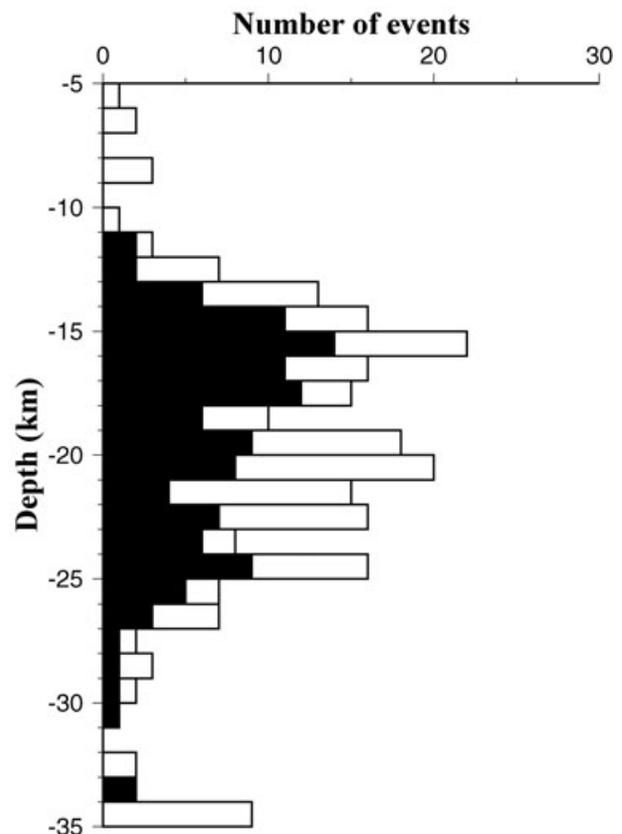

Figure 8. The depth distribution of aftershocks plotted as a histogram, showing both the high-quality (group A) locations in black and the lower-quality (group B) locations in white. Note the lack of high-quality depths shallower than 10 km, and the concentration of the high-quality depths close to the 22 km centroid depth of the mainshock.

of this depth are known in the circum-Caspian seismic belts, with confirmed depths as great as 27 km in the Talesh (see Section 2) and even deeper ones associated with the trans-Caspian Apscheron–Balkhan sill (Jackson *et al.* 2002; Engdahl *et al.* 2006). These are, nonetheless, the first confirmed depths as great as 30 km in the central Alborz, although some have been suspected from teleseismic locations (Engdahl *et al.* 2006). The mainshock centroid depth of 22 km, determined in Section 4, and four of the five hyocentral depths in Table 1, determined from arrival times, lie near the middle of the aftershock depth range.

Second, the complete lack of high-quality earthquake depths shallower than 10 km is remarkable. Even among the poorer-quality group B locations there are very few shallower than 10 km (Fig. 8), and these are probably unreliable. The station distribution is sufficiently dense, with two stations within the aftershock pattern itself (Fig. 6), for earthquakes shallower than 10 km to be detected and located, if they occurred. There is no reason to believe their absence is an artifact. The depth distribution observed here is, in some ways, reminiscent of the aftershock pattern of the 2003 Bam earthquake (Tatar *et al.* 2005; Jackson *et al.* 2006), where aftershocks were restricted to the depth range 8–20 km, also with no shallow events. But at Bam the aftershocks were almost entirely below the fault patch at 2–8 km depth that ruptured in the mainshock, whereas at Baladeh the mainshock centroid, and the probable hypocentral depth, lie right in the middle of the aftershock distribution itself. The geological contexts of the two earthquakes are also quite different: the Bam earthquake occurred in an intracontinental setting, whereas the Baladeh earthquake is located on the probable underthrust boundary between continental (the Alborz) and suspected oceanic (the South Caspian Sea) crusts, which we discuss more later.

Third, the aftershock distribution, though relatively dispersed and definitely not confined to a single plane, nonetheless clearly shows a zone dipping SSW (section A–AA, Fig. 7). This is the dip direction of the thrusts that outcrop on the northern flank of the Alborz range, including the Khazar, North Alborz and Kojour thrusts marked on Figs. 1 and 6. The deepest events, below 30 km, are all in the western part of the aftershock zone (section D–DD).

The significance of these observations will be discussed in the synthesis in Section 7.

6.3 Focal mechanisms

With only 10 seismic stations in the temporary network, first-motion fault plane solutions are not of the highest quality. We were able to determine 27 solutions, all of which had at least six first-motion polarities, none of them inconsistent with the nodal planes that we indicate. They are not well constrained, but are good enough to be able to distinguish those that involve thrust faulting, similar in nature to the mainshock, from strike-slip faulting. They are shown in Fig. 9. The most noteworthy feature of their distribution is that those in the east are mostly thrusts, whereas those in the west are mostly strike-slip, the majority (but not all) of the latter with one nodal plane striking roughly N–S. Their source parameters are listed in the Appendix (Table A1).

7 OVERVIEW OF FAULTING IN THE BALADEH EARTHQUAKE

The aftershock distribution is restricted between about 10 and 35 km depth (Figs 7 and 8). If we assume the co-seismic fault surface is contained entirely within this depth range, and is equidimensional,
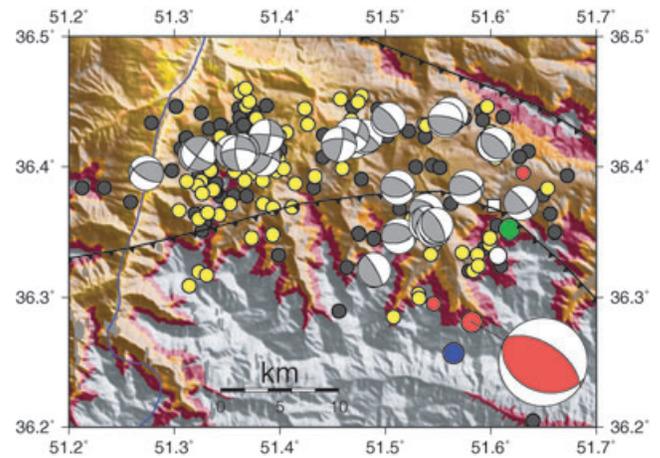
Figure 9. Lower-hemisphere fault plane solutions of selected aftershocks are plotted in gray (see text). The red focal sphere is that of the mainshock, plotted at the favoured mainshock epicentre determination. Yellow, gray, red, green, white and blue epicentres are those in Fig. 6. Black lines are the North Alborz (north) and Kojour (south) faults.

with down-dip width and along-strike length equal to L, we can estimate the source dimension, L, from the seismic moment, M_0, using the expression $L^3 = M_0/\mu\alpha$, where μ is the rigidity (approximately 3×10^{10} N m^{-2}) and α is the ratio of average coseismic displacement, $\bar{u}$, over length L. The value of α for intracontinental earthquakes is usually close to 5×10^{-5} (Scholz 1982), so if we take the moment value of 3×10^{18} N m from Section 4, we obtain an estimate for L of about 15 km.

For illustrative purposes, a coseismic fault surface of dimension 15×15 km^2 has been projected onto the cross sections in Fig. 7. In the across-strike section (A–AA) the fault, marked by a thick line, is centred at the centroid depth of 22 km, with the dip of $34°$ determined from teleseismic waveform modelling (Section 4). It is drawn on a downward projection from the topographic front (the 'Khazar thrust') with the same constant dip. In the along-strike section (D–DD) it has again been centred at 22 km depth, with its SE edge aligned with the trend of the five epicentre estimates in Table 1 and Fig. 6, which also corresponds with the SE edge of the aftershock distribution (Fig. 6). From this exercise, it is not surprising that the coseismic rupture plane failed to produce a scarp at the Earth's surface: it was clearly not big enough in area to do so, given its moment and depth.

If we assume that the topographic front really does mark the surface expression of a blind or through-going Khazar Fault, then the section A–AA in Fig. 7 also shows that an extrapolation of that fault to depth, using the dip of $34°$ determined for the Baladeh mainshock, passes through the south-dipping aftershock distribution and is consistent with the various mainshock hypocentre estimates, given their uncertainties. Thus our available information is consistent with the Khazar fault being the structure that slipped at depth in the 2004 Baladeh earthquake, and also with the Khazar fault continuing to at least 35 km depth. The Khazar fault as the source of the 2004 Baladeh earthquake would, perhaps, not be surprising, as it is by far the dominant geomorphological and structural feature in the epicentral region, marked by an abrupt topographic step (see topographic section in Fig. 7) and a limit to the incision of rivers flowing from the Alborz (Antoine *et al.* 2006). Nonetheless, the apparently perfect extrapolation in section A-AA of Fig. 7 is somewhat misleading, and we should recall the likely errors. The centroid depth of the

mainshock is uncertain by ±4 km and its hypocentral estimates by at least as much. Furthermore, the hypocentre marks, in principle, the onset of rupture, whereas the centroid is an averaged centre of the rupture surface. The hypocentre could, in principle, be anywhere within the aftershock distribution in Fig. 7. Nonetheless, in spite of these uncertainties, we should recall that the waveform analysis in Section 4 allows the fault dip to be up to about 10° *shallower* than the inversion value of 34° used in Fig. 7, but not significantly steeper. It is therefore very difficult to project the fault to the surface out-crop of either the North Alborz or Kojour thrust faults, the only other significant ones in the area. Thus the consideration of errors, as well as the geomorphology, lead us conclude that it was probably a part of the Khazar fault that moved, in a depth range of about 27–16 km. Both the lack of shallow aftershocks and the source dimensions suggest the Khazar fault did not slip seismically at depths less than about 10 km. Whether or not the North Alborz and Kojour thrusts are still active, and whether they merge, as splays, with the 2004 coseismic rupture surface at depth, are interesting issues, but not ones with which we have any information to address. Nor can we tell whether the Khazar fault is itself a steep splay off a flatter thrust that either separates the South Caspian basement from its sediments, or penetrates those sediments themselves (shown schematically, and at arbitrary depth, by the thin dotted line marked with a ? in Fig. 7). Clearly, the lack of shallow seismicity limits what we can say about the structure above 10 km depth. But the coincidence of the co-seismic rupture surface projecting to the topographic front at the Khazar 'thrust' remains a robust feature, and it is for that reason that we refer to the 2004 earthquake as being on the deeper part of the Khazar thrust in the remainder of this paper; aware that its shallower structure remains controversial.

The aftershock distribution in Figs 6 and 7 makes it likely that most of the aftershocks occurred around the edge of the coseismic slip surface, rather than on it, which is not unusual (e.g. Mendoza & Hartzell 1988; Bakun *et al.* 2005). In this case, the favoured epicentral location also suggests the rupture propagated to the west, and probably up-dip, though the earthquake was too small for this to be resolvable on the long-period seismograms of Fig. 3. In the west, where most aftershocks concentrate (Figs 6 and 7), the aftershocks seem to end nearly along the line of the Chalus river. This may indicate that the river follows a significant structural feature that inhibits rupture propagation on the Khazar thrust. The dominance of N–S strike-slip focal mechanisms in the western part of the aftershock zone (Fig. 9) is also consistent with a lateral ramp in the thrust surface, approximately aligned with the Chalus river. A similar feature suggested itself in the much bigger (M_w 7.3) Rudbar earthquake of 1990 in the Western Alborz. That earthquake involved a total of 80 km of left-lateral surface rupture in at least three distinct segments (Berberian *et al.* 1992). The Sefidrud river, the only river to flow right across the Alborz, crosses the line of these ruptures between two coseismic fault segments. The river is followed by a major road and a gas pipe-line, neither of which was cut by coseismic ruptures, even though a few km to either side the coseismic displacements were as much as 3 m. Thus the Sefidrud and Chalus rivers may both follow transverse geological structures that act as barriers to rupture propagation; though in both places the dense vegetation and high-erosion rates obscure the detailed geology, and this suggestion remains speculative.

Thus the available data allow us to assemble a self-consistent, coherent image of the coseismic faulting in the 2004 Baladeh earthquake. It remains to discuss briefly its significance for the geology of the Alborz and the seismic hazard in Tehran.

8 DEFORMATION OF SOUTH CASPIAN BASIN MARGIN AND THE ALBORZ

The 2004 Baladeh earthquake provides the first real information about the active geological structure at depth beneath the central Alborz. If we are right about the earthquake being on the deep part of the Khazar thrust, then an important feature is the lack of after-shocks shallower than 10 km, which might suggest that its shallower part is always aseismic. This would, in fact, not be surprising, when we consider that the geological function of the Khazar thrust is to push the crystalline igneous and sedimentary rocks of the Alborz over the great (probably 5–15 km) thickness of soft, overpressured muds and sands of the South Caspian Basin, which may well de-form aseismically at shallow depths (Jackson *et al.* 2002). In this respect, the Caspian margin in the central Alborz may resemble that of the Talesh, in the SW corner of the Caspian, where low-angle thrusts move seismogenically in the depth range 20–27 km, whereas the overpressured muds offshore deform aseismically in folds that are completely detached from the basement beneath (Jackson *et al.* 2002; Allen *et al.* 2003b; Vincent *et al.* 2005). There are no accurate local determinations of earthquake depths in the Talesh to examine the depth distribution in detail, but it would not be surprising if the top 10 km were aseismic, as in the central Alborz near Baladeh. The relatively aseismic nature of thrust faults at shallow depths, at least as far as larger earthquakes are concerned, is common in oceanic regions where thick sediments are being subducted, such as the Hellenic trench near Crete (Taymaz *et al.* 1990), and was illustrated recently in the 2005 Nias earthquake off Sumatra, where the coseismic slip patch was restricted to the depth range 14–35 km (Briggs *et al.* 2006), and the shallower part of the fault moved later by aseismic processes (Hsu *et al.* 2006). The same explanation has been offered for the lack of earthquakes shallower than 30 km on the trans-Caspian Apscheron–Balkhan sill (Jackson *et al.* 2002).

The Baladeh earthquake also offers insights to the 'partitioning' of the thrust and strike-slip components of deformation in the central Alborz. The well-determined slip vector of 036 ± 10° in the mainshock (Section 4) is clearly different from the NW–SE overall direction of shortening across the Alborz determined in GPS measurements by Vernant *et al.* (2004b). The missing component must be taken up by left-lateral faulting on the Taleghan, Mosha and Firuzkuh faults to the south, as surmised by a number of previous authors (Jackson *et al.* 2002; Allen *et al.* 2003a, 2004; Ritz *et al.* 2006). A cross-section across the Alborz is illustrative in this respect (Fig. 10). The Khazar fault, projected SW at 34° dip, does not intersect the vertical Mosha strike-slip fault within the seismogenic layer, even if that layer is 30 km thick across the whole range, which is unlikely. This relaxes considerably the kinematic constraints on their interaction, as movement on one does not offset the other; if they do intersect, they do so at greater depth, where ductile creep processes can overcome any space problems. This simple exercise shows that geological cross-sections of the Alborz that require the Khazar thrust to 'root' into the Mosha fault at shallow depths, resembling what is sometimes called a 'flower structure', are unlikely to be correct. They are based on the assumption that the Khazar fault flattens at shallow depth within the seismogenic layer, which the Baladeh earthquake shows is improbable. The unusually deep range of aftershock depths from the Baladeh earthquake is not likely to reflect a 'seismogenic thickness', in the usual sense of that term, on the north side of the Alborz. It is more likely to be related to the unusual circumstance of overthrusting thick, saturated
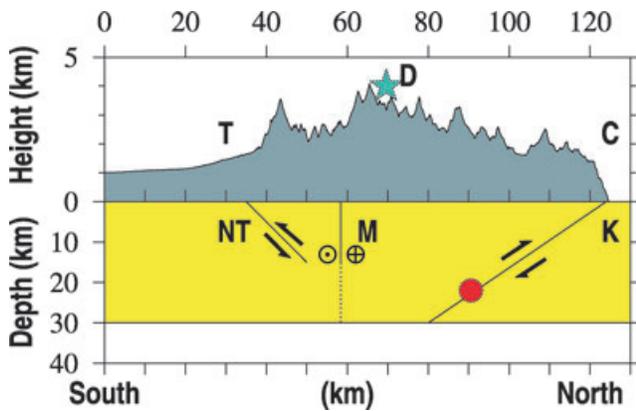
Figure 10. A section across the Alborz from near Tehran (T) at 35.5°N 51.3°E to near Chalus (C) at 36.8°N 51.8°E. The top is the vertically-exaggerated topography, shaded in gray. The blue star marked D is the projected position of Damavand volcano on this line of section. Beneath the topography, with equal vertical and horizontal scales, are shown the downward projections of the Khazar (K), Mosha (M) and North Tehran (NT) faults. The red circle is the approximate mainshock hypocentre (HDC epicentre plus 22 km centroid depth) for the 2004 Baladeh earthquake projected on to the line of section. The yellow layer is to illustrate a seismogenic layer 30 km thick: it does *not* represent the crustal thickness, which is about 40–50 km in the central Alborz. The aim is to show that even if the seismogenic layer was as thick as 30 km, the Khazar and Mosha faults are unlikely to intersect within the seismogenic layer. The North Tehran and Mosha faults may intersect within the seismogenic layer, depending on its thickness on the southern side of the Alborz and on the dip of the North Tehran Fault: see text for discussion.

sediments, which may not de-water sufficiently to allow frictional stick-slip until those greater depths. By contrast, Fig. 10 shows that the Mosha and North Tehran Faults might intersect within the seismogenic layer, even if that layer were only ~20 km thick, as it is in most other parts of Iran. To some extent, this will depend on the dip of the North Tehran fault, which is unknown (it is shown as 45° in Fig. 10, for illustrative purposes). Finally, Fig. 10 shows that the location of the Damavand stratovolcano, a Holocene trachyte-andesite edifice 5670 m high that dominates the skyline in this region, is located in such a position that need not interact with either the Mosha or Khazar faults, at least within the seismogenic layer.

9 IMPLICATIONS FOR SEISMIC HAZARD IN TEHRAN

As Fig. 2 makes clear, the historical earthquakes known to have affected the Tehran region have caused investigators to focus on the faults on the south side of the Alborz range; especially the Taleghan, Mosha and Firuzkuh strike-slip faults and the North Tehran Fault and its associated smaller thrusts. These undoubtedly do represent a formidable hazard. But the experience of the 2004 Baladeh earthquake, and the analysis of its generative fault given here, shows that some risk is also posed by faults on the north side of the Alborz, particularly the Khazar thrust. This is partly because the seismogenic depth extends quite deep (to ~35 km) on the north side, allowing slip patches to move further south than might otherwise have been anticipated. The 1957 July 2 (M_s 6.8) earthquake just east of Fig. 2, at approximately 36.05°N 52.45°E, also had a thrust mechanism (McKenzie 1972) and was a similar distance SW of the Khazar thrust to the 2004 Baladeh earthquake. It too, may have moved a

deep part of that thrust system, and was a significantly larger event. The large seismogenic depth on the north side can potentially lead to large down-dip widths, fault areas, and hence seismic moments in earthquakes; though the maximum earthquake size may in fact be limited by the top 10 km behaving aseismically and by structural interruptions to lateral rupture propagation, as we speculated above for both the 1990 Rudbar and 2004 Baladeh earthquakes. A further reason to fear earthquakes on the north side of the Alborz, in spite of their greater distance from Tehran than the faults on the south side, is that Tehran has become increasingly vulnerable to the long-period ground shaking through the steady increase in the size and elevation of its buildings. Long periods are less attenuated with distance than short periods, so that cities like Tehran, whose low-rise buildings were probably not much affected by earthquakes north of the Alborz in the past, now have high-rise buildings that are much more vulnerable to them. This is a situation common throughout the Mediterranean and Middle East.

10 CONCLUSIONS

The principal lesson to be drawn from the 2004 Baladeh earthquake is that it is not always the biggest earthquakes that are the most informative about a region. This single, moderate-sized earthquake, because it is the only one of modern times to occur in the central Alborz, has yielded a wealth of information about the tectonics and structure of that range. The biggest surprise is that co-seismic slip occurs as deep as ~35 km on the north side of the range, and that the the top 10 km may be deform aseismically, because of the thick pile of saturated sediments involved. The earthquake provided the first reliable slip vector azimuth in the area, which differs from the overall direction of shortening estimated from GPS, thereby confirming the spatial separation ('partitioning') of strike-slip and thrust components across the range inferred from geological evidence and seismicity in the east and west Alborz. The earthquake probably moved the frontal Khazar fault, which consequently must extend to a depth of at least 30–35 km and which does not need to mechanically interact with the partitioned strike-slip faulting south of it, at least within the seismogenic layer. If there is any such mechanical interaction between strike-slip and thrust faults, it is much more likely on the south side, between the North Tehran Fault system and the Mosha fault.

REFERENCES

Allen, M.B., Jones, S., Ismail-Zadeh, A. & Simmons, M.D., 2002. Onset of subduction as the cause of rapid Pliocene-Quaternary subsidence in the South Caspian Basin, *Geology,* **30,** 775–778.

Allen, M.B., Ghassemi, M.R., Shahrabi, M. & Qorashi, M., 2003a. Accommodation of late Cenozoic oblique shortening in the Alborz range, northern Iran, *J. Struct. Geol.,* **25,** 659–672.

Allen, M.B., Vincent, S.J., Alsop, G.I., Ismail-zadeh, A. & Flecker, R., 2003b. Late Cenozoic deformation in the South Caspian region: effects of a rigid basement block within a collision zone, *Tectonophysics,* **366,** 223–239.

Allen, M., Jackson, J. & Walker, R., 2004. Late Cenozoic reorganization of the Arabia-Eurasia collision and the comparison of short-term and long-term deformation rates, *Tectonics,* **23,** TC2008.

Ambraseys, N.N. & Melville, C.P., 1982. *A history of Persian earthquakes*, Cambridge University Press, UK, 219pp.

Antoine, P., Bahain, J., Berillon, G. & Khaneghah, A., 2006. Tuf calcaire et séquence alluviale en contexte tectonique actif: la formation de Baliran (province du Mazandaran, Iran), *Quaternaire,* **4,** 321–331.

Ashtari, M., Hatzfeld, D. & Kamalian, N., 2005. Microseismicity in the region of Tehran, *tectonophysics,* **395,** 193–208.

Axen, G.J., Lam, P.S., Grove, M. & Stockli, D.F., 2001. Exhumation of the west-central Alborz mountains, Iran, Caspian subsidence, and collision-related tectonics, *Geology,* **29,** 559–562.

Bakun, W.H. *et al.*, 2005. Implications for prediction and hazard assessment from the 2004 Parkfield earthquake, *Nature,* **437,** 969–974.

Berberian, M., 1983. The southern Caspian: a compressional depression floored by a trapped, modified oceanic crust, *Canad. J. Earth Sci.,* **20,** 163–183.

Berberian, M., 1994. Natural hazards and the first earthquake catalogue of Iran. Volume 1: Historical hazards in Iran prior to 1900, *Int. Inst. Earthquake Engineering and Seismology, Tehran,* 603pp.

Berberian, M., 2005. The 2003 Bam urban earthquake: a predictable seismotectonic pattern along the western margin of the rigid Lut block, southeast Iran, *Earthquake Spectra,* **21,** S35–S99.

Berberian, M., Qorashi, M., Arzhang-Ravesh, B. & Mohajer-Ashjai, A., 1985. Recent tectonics, seismotectonics and earthquake-fault hazard study of the Greater Tehran area. Contribution to the Seismotectonics of Iran, Part V, *Geol. Surv. Iran,* **56,** 316pp (in Persian).

Berberian, M., Qorashi, M., Jackson, J.A., Priestley, K. & Wallace, T., 1992. The Rudbar-Tarom earthquake of 20 June 1990 in NW Persia: preliminary field and seismological observations, and its tectonic significance, *Bull. seism. Soc. Am.,* **82,** 1726–1755.

BHRC: Building and Housing Research Center, 2004. Preliminary report on Baladeh-Kojour. Ministry of Housing and Unrban Development, Tehran. (Available on-line from http://www.bhrc.ac.ir)

Biggs, J., Bergman, E., Emmerson, B., Funning, G., Jackson, J., Parsons, B. & Wright, T., 2006. Fault identification in buried strike-slip earthquakes using InSAR: the 1994 and 2004 Al Hoceima, Morocco, earthquakes, *Geophys. J. Int.,* **166,** 1347–1362.

Bilham, R., 2004. Urban earthquake fatalities: a safer world, or worse to come? *Seismol. Res. Letts.,* **75,** 706–712.

Bondar, I., Myers, S.C., Engdahl, E.R. & Bergman, E.A., 2004. Epicentre accuracy based on seismic network criteria, *Geophys. J. Int.,* **156,** 1–14.

Briggs, R.W. *et al.*, 2006. Deformation and slip along the Sunda megathrust in the great 2005 Nias–Simeulue earthquake, *Science,* **311,** 1897–1901.

Copley, A. & Jackson, J., 2006. Active tectonics of the Turkish–Iranian plateau, *Tectonics,* **25,** TC6006.

Devlin, W.J., Cogswell, J.M., Gaskins, G.M., Isaksen, G.H., Pitcher, D.M., Puls, D.P., Stanley, K.O. & Wall, G.R.T., 1999. South Caspian basin: young, cool, and full of promise, *GSA today,* **9,** 1–9.

Engdahl, E.R., Jackson, J.A., Myers, S.C., Bergman, E.A. & Priestley, K., 2006. Relocation and assessment of seismicity in the Iran region, *Geophys. J. Int.,* **167,** 761–778.

Guest, B., Axen, G., Lam, P. & Hassanzadeh, J., 2006a. Late Cenozoic shortening in the west-central Alborz mountains, northern Iran, by combined conjugate strike-slip and thin-skinned deformation, *Geosphere,* **2,** 35–52.

Guest, B., Stockli, D., Grove, M., Axen, G., Lam, P. & Hassanzadeh, J., 2006b. Thermal histories from the central Alborz mountains, northern Iran: implications for the spatial and temporal distribution of deformation in northern Iran, *Geol. Soc. Am. Bull.,* **118,** 1507–1521.

Hsu, Y.-J. *et al.*, 2006. Frictional afterslip following the 2005 Nias-Imeulue earthquake, Sumatra, *Science,* **312,** 1921–1926.

Jackson, J., 2006. Fatal attraction: living with earthquakes, the growth of villages into megacities and earthquake vulnerability in the modern world, *Phil. Trans. Roy. Soc. Lond. Ser. A,* **364,** 1911–1925.

Jackson, J.A., Priestley, K., Allen, M. & Berberian, M., 2002. Active tectonics of the South Caspian Basin, *Geophys. J. Int.,* **148,** 214–245.

Jackson, J. *et al.*, 2006. Seismotectonic, rupture-process, and earthquake-hazard aspects of the 26 December 2003 Bam, Iran, earthquake, *Geophys. J. Int.,* **166,** 1270–1292.

Jordan, T.H. & Sverdrup, K.A., 1981. Teleseismic location techniques and their application to earthquake clusters in the south-central Pacific, *Bull. seism. Soc. Am.* **71,** 1105–1130.

Kissling, E., 1988. Geotomography with local earthquake data, *Rev. Geophys.,* **26,** 659–698.

Lee, W.H.K. & Lahr, J.C., 1972. HYPO71 (revised), a computer program for determining hypocenters, magnitude and first motion pattern of local earthquakes, *U.S. Geol. Surv. Open File Rep.,* 75–311.

McCaffrey, R. & Abers, J., 1988. *SYN3: A program for inversion of teleseismic body wave form on microcomputers*, Air Force Geophysical Laboratory Technical Report, AFGL-TR-88-0099, Hanscomb Air Force Base, Massachusetts.

McCaffrey, R. & Nábělek, J., 1987. Earthquakes, gravity, and the origin of the Bali Basin: an example of a nascent continental fold-and-thrust belt, *J. geophys. Res.,* **92,** 441–460.

McCaffrey, R., Zwick, P. & Abers, G., 1991. *SYN4 Program*, IASPEI Software Library, **3,** 81–166.

McKenzie, D., 1972. Active tectonics of the Mediterranean region, *Geophys. J. R. astr. Soc.,* **30,** 109–185.

Mendoza, C. & Hartzell, S.H., 1988. Aftershock patterns and mainshock faulting, *Bull. seism. Soc. Am.,* **78,** 1438–1449.

Molnar, P. & Lyon-Caen, H., 1989. Fault plane solutions of earthquakes and active tectonics of the Tibetan Plateau and its margin, *Geophys. J. Int.,* **99,** 123–153.

Nábělek, J., 1984. Determination of earthquake source parameters from inversion of body waves, *PhD thesis*, MIT, Cambridge, MA.

Nazari, H. *et al.*, 2007. Paleoseismological analysis of the North Tehran Fault, Iran, *J. geophys. Res.,* submitted.

Parsons, B., Wright, T., Rowe, P., Andrews, J., Jackson, J., Walker, R., Khatib, M. & Talebian, M., 2006. The 1994 Sefidabeh (eastern Iran) earthquakes revisited: new evidence from satellite radar interferometry and carbonate dating about the growth of an active fold above a blind thrust fault, *Geophys. J. Int.,* **164,** 202–217.

Ritz, J.-F., Nazari, H., Ghassemi, A., Salamati, R., Shafei, A., Soleymani, S. & Vernant, P., 2006. Active transtension inside Central Alborz: a new insight into northern Iran—southern Caspian geodynamics, *Geology,* **34,** 477–480.

Scholz, C., 1982. Scaling laws for large earthquakes: consequences for physical models, *Bull. seism. Soc. Am.,* **72,** 1–14.

Sodoudi, F., Kind, R., Kamalian, N. & Sadidkhoy, A., 2004. The crustal and upper mantle structure of the central Alborz using teleseismic receiver functions, European Geosciences Union, 1st General Assembly, Nice, 25–30 April, 2004.

Tatar, M., Hatzfeld, D., Moradi, A.S. & Paul, A., 2005. The 2003 December 26 Bam earthquake (Iran), M_w 6,6, aftershock sequence, *Geophys. J. Int.,* **163,** 90–105.

Taymaz, T., Jackson, J. & Westaway, R., 1990. Earthquake mechanisms in the Hellenic Trench near Crete, *Geophys. J. Int.,* **102,** 695–731.

Taymaz, T., Jackson, J. & McKenzie, D., 1991. Active tectonics of the north and central Aegean Sea, *Geophys. J. Int.,* **106,** 433–490.

Vernant, Ph. *et al.*, 2004a. Contemporary crustal deformation and plate kinematics in Middle East constrained by GPS measurements in Iran and northern Oman, *Geophys. J. Int.,* **157,** 381–398.

Vernant, P. *et al.*, 2004b. Deciphering oblique shortening of central Alborz in Iran using geodetic data, *Earth planet. Sci. Lett.,* **223,** 177–184.

Vincent, S.J. Allen, M.B., Ismail-Zadeh, A.D., Flecker, R., Foland, K.A. & Simmons, M.D., 2005. Insights from the Talysh of Azerbaijan into the Paleogene evolution of the South Caspian region, *Geol. Soc. Am. Bull.,* **117,** 1513–1533.

Walker, R., Bergman, E., Jackson, J., Ghorashi, M. & Talebian, M., 2005. The 22 June 2002 Changureh (Avaj) earthquake in Qazvin province, NW Iran: epicentral re-location, source parameters, surface deformation and geomorphology, *Geophys. J. Int.,* **160,** 707–720.

Zanchi, A., Berra, F., Mattei, M., Ghassemi, M. & Sabouri, J., 2006. Inversion tectonics in central Alborz, Iran, *J. Struct. Geol.,* **28,** 2023–2037.

Zwick, P., McCaffrey, R. & Abers, G., 1994. *MT5 Program*, IASPEI Software Library, **4**.

APPENDIX A: AFTERSHOCK FAULT PLANE SOLUTIONS

Table A1. Source parameters of the aftershocks whose fault plane solutions are shown in Fig. 9. Depth (z) is in km.

Num	Date	Time	Lat.	Lon.	z	Str.	Dip	Rake
154	040605	00:10	36.410	51.371	17	290	70	27
156	040605	01:58	36.395	51.273	15	120	65	120
159	040605	20:58	36.406	51.384	22	285	70	141
161	040605	22:12	36.420	51.471	22	280	70	133
163	040606	02:20	36.384	51.577	12	75	55	59
165	040606	06:08	36.423	51.387	15	−85	80	163
166	040606	17:20	36.417	51.603	18	305	60	87
174	040607	04:01	36.423	51.481	18	305	75	90
182	040608	00:54	36.347	51.513	19	75	60	66
183	040608	01:13	36.412	51.364	15	−75	82	147
184	040608	01:58	36.409	51.320	16	125	75	−161
185	040608	02:24	36.410	51.323	15	125	75	0
186	040608	09:06	36.321	51.489	24	330	80	90
187	040608	10:46	36.424	51.468	16	30	70	14
189	040608	19:59	36.366	51.539	17	90	40	61
190	040608	22:41	36.356	51.539	21	330	70	90
191	040609	00:51	36.411	51.355	15	30	70	−14
193	040609	02:30	36.384	51.512	19	80	45	59
204	040610	22:01	36.410	51.361	16	175	75	−22
206	040611	12:18	36.352	51.546	21	330	70	90
208	040611	18:18	36.417	51.456	16	10	75	28
214	040612	06:43	36.436	51.503	14	320	70	101
216	040612	17:12	36.355	51.548	21	330	70	90
226	040612	21:31	36.440	51.562	19	305	75	90
228	040612	21:49	36.436	51.557	17	280	75	90
233	040614	00:13	36.372	51.629	26	60	50	15
240	040615	20:31	36.417	51.604	17	310	60	87